INL/CON-08-14907
PREPRINT

Development and Validation of a Multifield Model of Churn-Turbulent Gas/Liquid Flows

ICONE 17

Elena A. Tselishcheva
Donna Post Guillen
Steven P. Antal
Matthias Beyer
Michael Z. Podowski
Dirk Lucas

July 2009

The INL is a
U.S. Department of Energy
National Laboratory
operated by
Battelle Energy Alliance

Proceedings of the 17th International Conference on Nuclear Engineering
ICONE17
July 12-16, Brussels, Belgium

ICONE17-75210

DEVELOPMENT AND VALIDATION OF A MULTIFIELD MODEL OF CHURN-TURBULENT GAS/LIQUID FLOWS

Elena A. Tselishcheva
Center for Multiphase Research
Rensselaer Polytechnic Institute
Troy, NY, USA

Steven P. Antal
Center for Multiphase Research
Rensselaer Polytechnic Institute
Troy, NY, USA

Michael Z. Podowski
Center for Multiphase Research
Rensselaer Polytechnic Institute
Troy, NY, USA

Donna Post Guillen
Idaho National Laboratory
Idaho Falls, Idaho, USA

Matthias Beyer
Forschungszentrum Dresden-Rossendorf e.V. Institute of Safety Research
Dresden, Germany

Dirk Lucas
Forschungszentrum Dresden-Rossendorf e.V. Institute of Safety Research
Dresden, Germany

ABSTRACT

The accuracy of numerical predictions for gas/liquid two-phase flows using Computational Multiphase Fluid Dynamics (CMFD) methods strongly depends on the formulation of models governing the interaction between the continuous liquid field and bubbles of different sizes. The purpose of this paper is to develop, test and validate a multifield model of adiabatic gas/liquid flows at intermediate gas concentrations (e.g., churn-turbulent flow regime), in which multiple-size bubbles are divided into a specified number of groups, each representing a prescribed range of sizes. The proposed modeling concept uses transport equations for the continuous liquid field and for each bubble field. The overall model has been implemented in the NPHASE-CMFD computer code. The results of NPHASE-CMFD simulations have been validated against the experimental data from the TOPFLOW test facility. Also, a parametric analysis on the effect of various modeling assumptions has been performed.

INTRODUCTION

One of the most important and yet least understood aspects of two-phase flow is concerned with the lateral phase distribution mechanisms, especially for situation when bubbles of different sizes and concentrations interact with the liquid and with other bubbles. The major purpose of this paper is to develop a physically-consistent model of bubble/liquid interactions. The flow conditions of reference are based on the experimental data obtained at the TOPFLOW test facility at Forschungszentrum Dresden-Rossendorf e.V. Institute of Safety Research [Prasser et al, 2007]. Details concerning the experimental setup and results are given in a separate section of this paper. An important feature of the TOPFLOW experiments was that it allowed one to identify local distributions of the volume fractions of bubbles in each of four different bubble size groups. This, in turn, served as a reference for testing a three-dimensional five-field model of two-phase flow. Due to the axial symmetry of the experimental results, the computer simulations performed in this work have been focused on the radial and axial distributions of major flow parameters.

The simulations were performed using a state-of-the-art computational multiphase fluid dynamics code, NPHASE–CMFD [Antal et al.,2000]. A complete five-field model, including the continuous liquid field and four dispersed fields representing bubbles of different sizes, was first carefully tested for numerical convergence and accuracy, and then used to reproduce the experimental results of TOPFLOW. Since the closure laws employed in the present multifield modeling concept allow for adjusting selected parameters, a parametric study was also performed to assess the sensitivity of predictions to major modeling assumptions.

NOMENCLATURE

D	Diameter (m)
d_b	Diameter of bubble (mm)
i,j,k	Numerical indexes
J	Superficial velocity (m/s)
l,g	Indexes for liquid and gas respectively
L	Length (m)
P	Pressure (Pa)

$\mathbf{v}$	Velocity vector (m/s)
x,y,z	Coordinates
α	Volumetric gas fraction
m'''	Volumetric mass transfer between fields representing the same phase
$\mathbf{M}$	Interfacial force per unit volume (N/m^3)
τ	Shear stress
$\mathbf{g}$	Acceleration of gravitation (m/s^2)
ρ	Density (kg/m^3)
A'''	Interfacial area density (1/m)
u_{rel}	Relative velocity of the dispersed field (m/s)
Re	Reynolds Number
μ	Viscosity (kg/m-s)

MODEL FORMULATION

The multifield model of multiphase/multicomponent flows of interpenetrating fluids is based on ensemble averaging the equations governing the mass, momentum and energy conservation for each field. Such modeling, with appropriate closure laws, is capable of capturing flow regimes from bubbly through churn-turbulent and slug, to annular flow. A general form of the multifield equations for adiabatic flows is [Podowski, 2009]

Mass conservation

$$\frac{\partial(\alpha_k\rho_k)}{\partial t}+\nabla\cdot(\alpha_k\rho_k\mathbf{v}_k)=m_k''' \tag{1}$$

Momentum conservation

$$\begin{aligned}&\frac{\partial\ \alpha_k\rho_k\mathbf{v}_k}{\partial t}+\nabla\cdot\ \alpha_k\rho_k\mathbf{v}_k\mathbf{v}_k\ =-\alpha_k\nabla p_k\\&-\sum_j\ p_k-p_{kj}^j\ \nabla\alpha_j+\alpha_k\nabla\cdot\underline{\underline{\tau}}_k+\sum_j\ \underline{\underline{\tau}}_k-\underline{\underline{\tau}}_{kj}^i\ \nabla\alpha_j\\&+\alpha_k\rho_k\mathbf{g}+\sum_j\mathbf{M}_{kj}^i+\sum_m m_{m,k}'''\mathbf{v}_m^i\end{aligned} \tag{2}$$

where $m_k'''=\sum_m m_{m,k}'''$.

In Eqs.(1) and (2), α_k is the volumetric fraction of field-k, m_k''' is the volumetric mass transfer term into field-k from other fields representing the same phase, $\mathbf{M}_{kj}^i$ is the interfacial momentum transfer per unit time (interfacial force) between fields k and j, $\underline{\underline{\tau}}_k=\underline{\underline{\tau}}_k^{\mu}+\underline{\underline{\tau}}_k^{\mathrm{Re}}$ is the total shear stress term, the subscript 'i' refers to interfacial variables, and the remaining notation is conventional.

As it has been shown by Podowski [2009], the multifield approach can be used as a practical engineering model approximation for dispersed 'particle' flows, such as gas/liquid two-phase flows. Since individual particles are not in contact with one another and no forces of any kind (neither pressure nor shear) can be transmitted between them, the dispersed particles do not represent a distinct "field". Thus, additional assumptions must be made to convert the dispersed particle momentum equation into a full-field form. In particular, taking $\underline{\underline{\tau}}_{kj}^i=\underline{\underline{\tau}}_{d,k}=\underline{\underline{\tau}}_c=\underline{\underline{\tau}}$ and $p_k^i=p_{d,k}=p_c=p$, yields a consistent multifield formulation of the multiple-bubble-size model of two-phase flows. The corresponding momentum equation for an arbitrary (continuous or dispersed) field-k becomes

$$\begin{aligned}&\frac{\partial\ \alpha_k\rho_k\mathbf{v}_k}{\partial t}+\nabla\cdot\ \alpha_k\rho_k\mathbf{v}_k\mathbf{v}_k\ =-\alpha_k\nabla p\\&+\alpha_k\nabla\cdot\underline{\underline{\tau}}+\alpha_k\rho_k\mathbf{g}+\mathbf{M}_k^i+\sum_m m_{m,k}'''\mathbf{v}_m^i\end{aligned} \tag{4}$$

The model given by Eq.(1) and Eq.(4) is applicable to general time-dependent or steady-state developing flow situations. Since, as it is discussed in the following Sections, the selected TOPFLOW data refer to nearly-fully-developed flow conditions, and both phases can be treated as incompressible, the governing equations for mass and energy used as a basis for model validation simplify to the following respective forms

$$\alpha_k\mathbf{v}_k=constant \tag{5}$$

$$-\alpha_k\nabla p+\alpha_k\nabla\cdot\underline{\underline{\tau}}+\alpha_k\rho_k\mathbf{g}+\mathbf{M}_k^i=0 \tag{6}$$

Furthermore, given the circular tube geometry and vertical orientation of the TOPFLOW test section, and the axial symmetry of average flow parameters, the assessment of predictive capabilities of the current model is mainly associated with the radial component of Eq.(6), i.e.

$$0=-\alpha_k\frac{\partial p}{\partial r}+\alpha_k\frac{\partial}{\partial r}\left(\mu_l'\frac{\partial \mathrm{v}_l}{\partial r}\right)+M_{r,k}^i \tag{7}$$

Since for such flow conditions, the radial pressure gradient and radial velocity component are practically both equal to zero, the radial momentum equation reduces to the interfacial force balance

$$M_{r,k}^i=0\quad\text{for}\quad k=1,...,N \tag{8}$$

It is commonly assumed that, in general, the total interfacial force on phase-k can be expressed as a superposition of several component forces [Drew, 1992]

$$\mathbf{M}_k^i=\sum_j\mathbf{M}_{kj}^i \tag{9}$$

where the individual components represent forces such as, drag, virtual mass, lift, and other interfacial forces.

In the present model, the overall multidimensional interfacial force is given by

$$\mathbf{M}_k^i=\mathbf{M}_k^D+\mathbf{M}_k^{VM}+\mathbf{M}_k^{TD}+\mathbf{M}_k^L+\mathbf{M}_k^W \tag{10}$$

where $\mathbf{M}_k^D$ is the drag force, $\mathbf{M}_k^{VM}$ is the virtual mass force, $\mathbf{M}_k^{TD}$ is the turbulent dispersion force, $\mathbf{M}_k^L$ is the lift force and $\mathbf{M}_k^W$ is the wall force.

In general, closure laws are flow-regime dependent. For churn-turbulent flows, the expressions for interfacial forces are based on the interaction between individual bubbles and the surrounding them continuous liquid. However, due to the differences in both bubble size and shape, the coefficients used to quantify the various forces may vary from one field to another.

In fully-developed flows, the virtual mass force reduces to zero, and so does the radial component of drag force. The axial component of the drag force can be written as

$$M_{r,v_k-l}^D = -\frac{1}{8} C_{D,k} A_{i,k}''' \rho_l \left| u_{rel,k} \right| u_{rel,k} \tag{11}$$

where $A_{i,k}'''$ is the interfacial area density, $C_{D,k}$ is the drag force coefficient, and $u_{rel,k}$ is the relative velocity, all of the *k*-th dispersed field.

In the present model, the drag coefficient is given by the expression proposed by Wallis [1969]

$$C_{D,k} = \begin{cases} \dfrac{24}{Re_{p,k}} \left[1 + 0.1 Re_{p,k}^{\,0.75} \right] & for \;\; Re_{p,k} \le 1000 \\ 0.44 & for \;\; Re_{p,k} > 1000 \end{cases} \tag{12}$$

where $Re_{p,k}$ is the relative Reynolds number for group-*k* bubbles

$$Re_{p,k} = \frac{\rho_l u_{rel,k} d_{b,k}}{\mu_l} \tag{13}$$

and $d_{b,k}$ s the equivalent diameter of the respective bubble group.

Since at fully developed flow conditions the axial components of all interfacial forces other than drag get reduced to zero, the force balance in the upward direction for each dispersed field-*k* becomes

$$\alpha_k \;\; 1-\alpha \;\; (\rho_l - \rho_v) g = \frac{1}{8} C_{D,k} \rho_l A_{i,k}''' \left| u_{rel,k} \right| u_{rel,k} \tag{14}$$

where $\alpha = \sum_{k=1}^{N_d} \alpha_k$ is the local void fraction.

Hence, the liquid axial momentum equation represents a local balance between the drag force, gravity and buoyancy forces.

In the radial direction, the force balance for each dispersed field becomes

$$M_{r,k}^{TD} + M_{r,k}^L + M_{r,k}^W = 0 \tag{15}$$

In Eq.(15), the turbulent dispersion force is given by [Lopez de Bertodano, 1992]

$$M_k^{TD} = -C_{TD,k} \rho_c \kappa \frac{\partial \alpha_k}{\partial r} \tag{16}$$

where C_{TD} is turbulent dispersion coefficient and κ is the turbulent kinetic energy.

The wall force is modeled as

$$M_{l-v_k}^W = -C_{W,k} \rho_l \alpha_k \frac{\left| \mathbf{v}_{v,k} - \mathbf{v}_l \right|^2}{d_{b,k}} \tag{17}$$

The purpose of introducing the wall force was to account for the observed sudden decrease in bubble volumetric concentration very close to channel wall.

The expression used for wall force coefficient C_W [Antal et al., 2005] is

$$C_W = \begin{cases} 0.05 \left[1 + \left(\dfrac{y_w}{d_b} \right)^2 (2 \dfrac{y_w}{d_b} - 3) \right] & \text{for } y < d_b \\ 0 & \text{for } y \ge d_b \end{cases} \tag{18}$$

The interfacial lift force is used to account for the interfacial momentum exchange between the bubbles and the liquid field and can be written as

$$M_k^L = -C_{L,k} \rho_c \alpha_k u_{rel,k} \frac{\partial u_l}{\partial r} \tag{19}$$

Substituting Eqs.(16)-(19) into Eq.(15), yields the following form of the radial momentum equation for dispersed field-*k*

$$\begin{aligned} &-C_{TD,k} \rho_c \kappa \alpha_k \frac{\partial \alpha_k}{\partial r} + C_{W,k} \rho_l \alpha_k \frac{\left| \mathbf{v}_{v,k} - \mathbf{v}_l \right|^2}{d_{b,k}} \\ &-C_{L,k} \rho_c \alpha_k u_{rel,k} \frac{\partial u_l}{\partial r} = 0 \end{aligned} \tag{20}$$

A similar approach was used by [Lucas et al., 2001] for a first analysis using the Tomiyama lift force correlation [Tomiyama 1998] for poly-dispersed flows. The use of different models for bubble forces is discussed by [Lucas et al., 2007].

The effect of flow turbulence has been accounted for using the High Reynolds number k-ε model for the continuous liquid field, combined with the bubble-induced turbulence model proposed by Sato and Sekoguchi [1975].

The total effective viscosity in the liquid component of two-phase flow is normally given by

$$\nu_c^T = \nu_c^m + \nu_c^t + \nu_c^{2\phi} \tag{21}$$

where ν_c^m is the molecular kinematic viscosity of the liquid, $\nu_c^t = \dfrac{C_\mu \kappa^2}{\varepsilon}$ is the turbulent shear-induced kinematic viscosity, and $\nu_c^{2\phi}$ is the bubble-induced viscosity, and ε is the turbulent energy dissipation rate.

The conservation equations for the turbulent energy and energy dissipation rate, respectively, can be written as

$$\alpha_c \frac{Dk}{Dt} = \nabla \cdot \left(\frac{\alpha_c \nu_c^T}{\sigma_k} \nabla k \right) + \alpha_c \left(P_c - \varepsilon_c \right) \tag{22}$$

$$\alpha_c \frac{D\varepsilon_c}{Dt} = \nabla \cdot \left(\frac{\alpha_c \nu_c^T}{\sigma_\varepsilon} \nabla \varepsilon_c \right) + \alpha_c \frac{\varepsilon_c}{k_c} \left(P_c C_{1\alpha} - C_{2\alpha} \varepsilon_c \right) \tag{23}$$

The bubble-induced kinematic viscosity of the liquid phase is given by [Sato and Sekoguchi, 1975]

$$\nu_c^{2\phi} = \sum_{k=1}^{N_d} C_{\mu b} d_{d,k} \alpha_k \left| u_{rel,k} \right| \tag{24}$$

The following standard values of the coefficients in Eqs.(21) through (24) have been used in the present model: C_μ=0.09, $C_{1\alpha}$=1.44, $C_{2\alpha}$=1.92, σ_k=1.0, σ_ε=1.3, $C_{\mu b}$=1.2.

EXPERIMENTAL SETUP AND CONDITIONS

As it was mentioned before, the experimental data used for the validation of the present model have been taken at the thermal-dynamic test facility TOPFLOW [Schaffrath et al., 2001; Prasser et al.,2007] at the Institute of Safety Research of Forschungszentrum Rossendorf e.V. The name, TOPFLOW, is an acronym for transient TwO Phase FLOW. The test facility is designed for generic and applied studies of transient two-phase flow phenomena in power and process industries.

The TOPFLOW facility is equipped with two vertical test sections, which are stainless steel pipes with inner diameters of 195.3 mm (DN200) as well as 52.3 mm (DN50). Both sections have a total height of 9 m. The flow rates in the test section DN200 (see Fig.1) may be assigned over the following range: the superficial gas velocity (j_v) between 0.0025 and 7.772 m/s, and the superficial liquid velocity (j_l) from 0.0405 to 1.61 m/s. Desalinated water was used in the experiments. The metering system for the injected air flow supplied volumetric flow rates related to standard conditions (p=1.013 bar, T=20°C). The data used for comparison have been obtained at L/D=40, where the flow was nearly fully developed. The test section DN200 is equipped with six gas injection locations which allow for injecting air or steam via orifices in the pipe wall. This gas injection via wall orifices offers the advantage that the two-phase flow can rise smoothly to the measurement plane, without being influenced by the feeder within the tube at any other locations along the flow. The inlet part of the test section is connected to a gas injection pipe and a compressed air system. The liquid phase is supplied from the bottom of the test section by means of an isolation valve and a 90° bend. The measurement plane was always situated at the upper end of the test section shown in Fig. 1.

Two wire-mesh sensors were used. While all data on gas volume fraction profiles and bubble size distributions were obtained from the lower (upflow) sensor, the second sensor was used to determine profiles of the gas velocity by cross-correlation measurements between the two sensors. Details on data evaluation and uncertainties of wire-mesh sensor measurements can be found in [Prasser et al., 2007a]. The errors of the wire-mesh sensor measurements for the gas fraction and bubble size have been mainly caused by the lateral pitch of the wires, which is 3 x 3 mm, and the distance of the wire planes, which is 2 mm. Comparative measurements between the wire-mesh sensor and other research methods supplied information on the accuracy of the measurement technique and the evaluation algorithms for the experimental determination of main flow parameters. The accuracy of the gas volume fraction averaged over the flow cross-section depends on the two-phase flow regime. Differences in the absolute void fraction were determined [Prasser et al. 2007] for bubbly flows in the range of ± 1 %, and a systematic underestimation of approx. - 4 % was observed for slug flows.

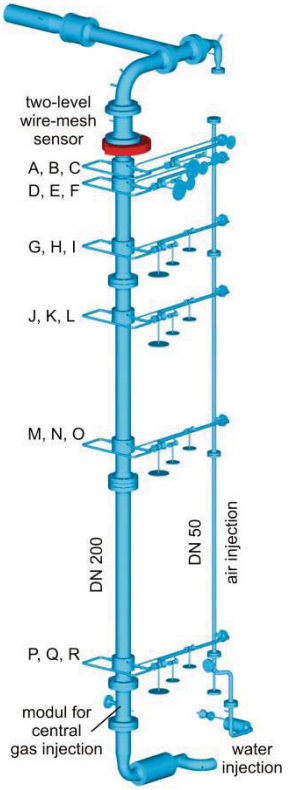

Figure. 1 Vertical test section of the TOPFLOW facility with variable gas injection system (DN 200).

The database established during the experiment contains CFD-grade data for the evolution of the flow along the pipe, including radial profiles of the void fraction and gas velocity, as well as bubble size distributions. The radial profiles of gas volume fraction for Run 118 are shown in Figure 2. These results were obtained for the water superficial velocity, j_l=1 m/s, and air superficial velocity, j_g=0.22m/s. As can be seen, the void concentration profiles near the exit of the test section

are almost independent of the axial position. This, in turn, show the flow is nearly fully developed in this region.

The flow regime attributed to the conditions shown in Figure 2 is churn-turbulent. All four bubble size classes initially experience a maximum close to the wall. Eventually, the peak disappears completely for bubbles larger than d_b = 5.8mm, while smaller bubbles maintain a wall peak over the entire axial distance along the flow. For small bubbles, between 0 and 4.8 mm in diameter, the wall peak is most pronounced and never diminishes, which confirms that the lift force is able to push small bubbles towards the wall even under the conditions of a churn-turbulent flow. All radial profiles reach quasi-equilibrium at L/D= 12.7.

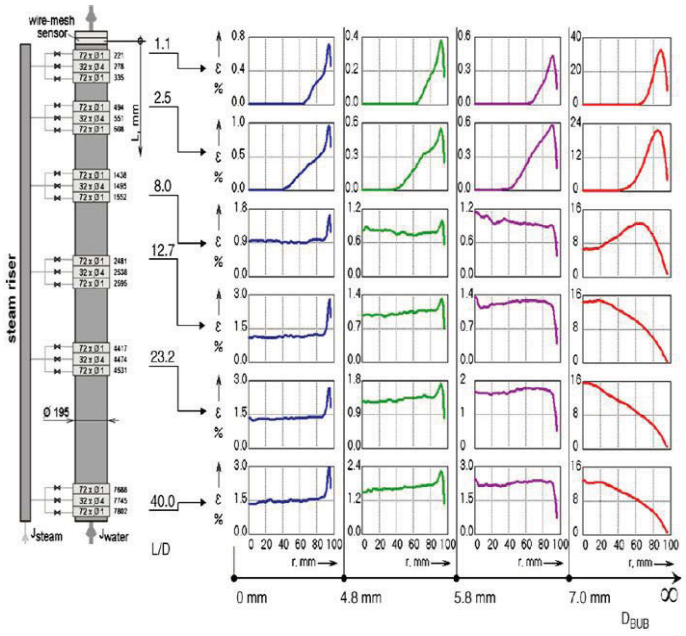

Figure 2. Gas volumetric fraction profiles decomposed according the bubble size classes, in the test pipe DN200 for an air/water experiment at j_l=1m/s and j_g=0.22m/s (from Prasser et al. 2007).

FORMULATION OF NPHASE-CMFD BASED COMPUTATIONAL MODEL

Overview of the NPHASE-CMFD Computer Code

The NPHASE-CMFD code [Antal et al, 2000] is a robust computational multiphase fluid dynamics (CMFD) flow solver. The technology used by the NPHASE code is the ensemble averaged multifield model of two-phase flows. Separate equations for the conservation of mass, momentum and energy for each fluid/field are developed as the framework. The governing equations are then ensemble averaged which allows the NPHASE-CMFD code to predict a time-average hydraulic performance. Key features of NPHASE-CMFD code are:

- Use of unstructured grids with arbitrary element types.
- Capability to model an arbitrary number of fields (fluid components and/or phases).
- Built-in mechanistic modeling, integrated with numerics.
- Improved robustness and numerical convergence.
- Free surface modeling.

Computational Grid and Boundary Conditions

The basic calculations presented in this paper were performed for a vertical circular tube with 24 uniformly distributed radial grid cells. A sample grid is shown in Figure 3. GRIDGEN was used as a computational grid generator, to build the desired mesh and specify the necessary boundary conditions. The length of the channel was, L= 16 m, and its diameter was, D = 0.194 m. The results of calculations used for the purpose of comparison with the TOPFLOW Test 118 data were obtained near the outlet of the pipe. This location corresponds to fully-developed flow conditions.

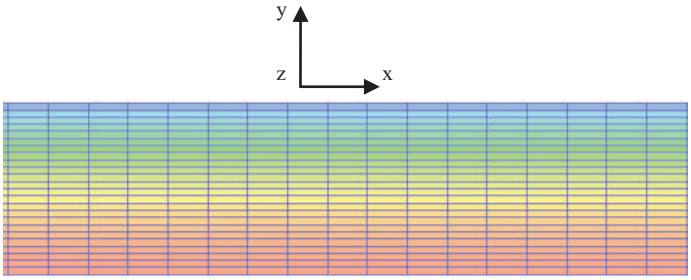

Figure 3. Schematic of grid geometry used in NPHASE-CMFD simulations.

The inlet conditions in the experimental test were j_g = 0.22 m/s and j_l = 1 m/s. Because of the lack of specific data, it has been assumed in the simulations that both liquid and gas enter the test section with an average velocity, u_{in} = 1.2 m/s. It should be pointed out here, that this assumption does not affect the flow conditions predicted at the exit of the test section.

According to the experimental results, the overall bubble population was divided into four groups. The average bubble diameter in each group represented the following range of sizes:

Group-1 (size range from 0 to 4.8 mm): d_1 = 3 mm,
Group-2 (size range from 4.8 mm to 5.8 mm): d_2 = 5 mm,
Group-3 (size range from 5.8 mm to 7 mm): d_3 = 6 mm,
Group-4 (sizes larger than 7 mm): d_4 = 10 mm.

Parametrically testing has shown that the differences between the results obtained using the integer values of bubble diameters given above and the arithmetic averages over each range are negligible.

MODEL VALIDATION AND TESTING

Two series of calculations have been performed. In the first series, fixed values of coefficients in all interfacial laws were assumed, based on the best available information and the experience from previous studies. Then, a parametric study was performed, to assess the sensitivity of predictions to the various modeling assumptions used. The results for both series are discussed next.

Base-Case Simulations

The initial conditions of the chosen sample experimental test were, j_g=0.22 m/s and j_f=1 m/s, which corresponds to a uniform inlet velocity, u_{in} = 1.2 m/s and an inlet average void fraction, α=0.18.

Figures 4, 5 and 6 show a comparison between the NPHASE-CMFD simulations and the TOPFLOW experimental data. Figures 4(a)-4(d) presents the radial void fraction profiles of bubbles of different average diameters. All profiles are plotted against the void distributions for the corresponding bubble size classes in the experimental tests.

As can be seen in Figures 4(a)-4(c), for all three groups of small bubbles, their concentrations experience wall peaking. For the case of large deformed bubbles, shown in Figure 4(d), the effect of lift force is opposite to that for small bubbles, so that the bubbles are pushed from the wall toward the center of the pipe.

Figure 5 shows the total void fraction distribution in the radial direction, as compared with the experimental data. As can be seen, the NPHASE-CMFD predictions are in good agreement with the measurements.

Figure 6 shows the velocity distributions for all five fields (liquid and four bubble groups), as well as the average gas velocity distribution. The latter has been compared against the only measured (average) flow velocity. Again, the agreement between the predictions and data is quite good.

In summary, whereas the NPHASE-CMFD results are in good agreement with the TOPFLOW data, there are several modeling issues, mainly associated with choice of lift coefficient for the various bubble sizes and other assumed parameters, where a parametric analysis can provide important insight into the sensitivity of the results of simulations to the various modeling and computational assumptions. The results of such a study are discussed next.

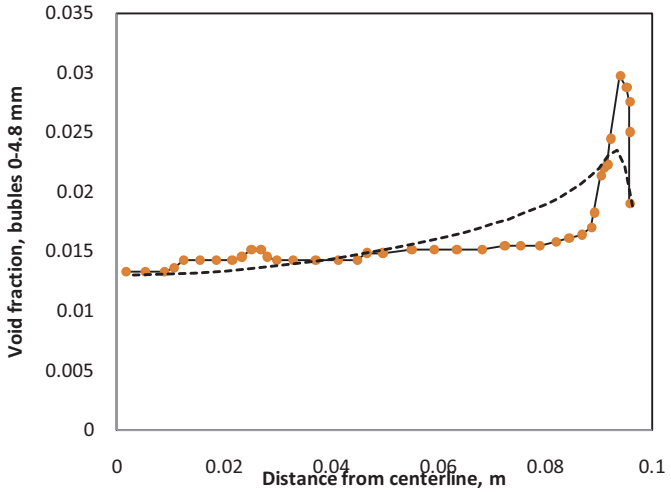

Figure 4(a). Radial distribution of volumetric concentration of bubbles having diameters between 0 and 4.8 mm.

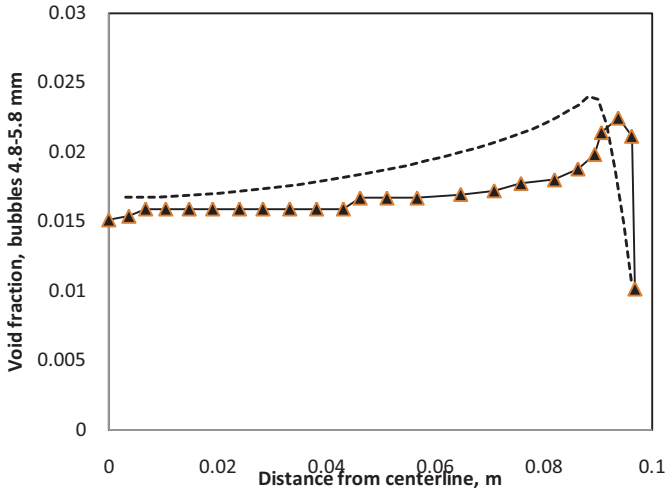

Figure 4(b). Radial distribution of volumetric concentration of bubbles having diameters between 04.8 and 5.8 mm.

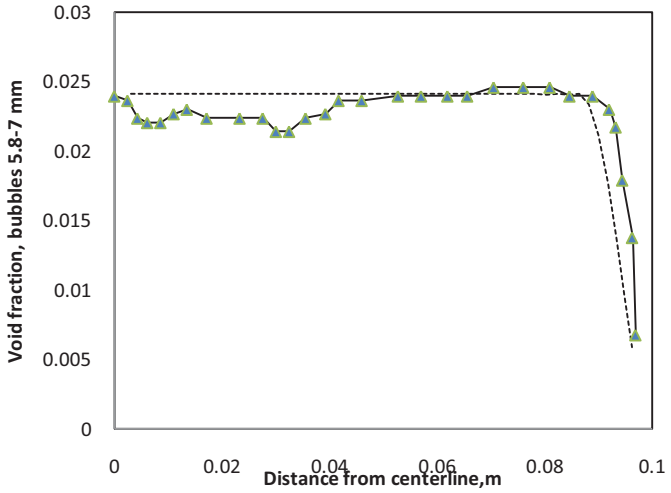

Figure 4(c). Radial distribution of volumetric concentration of bubbles having diameters between 5.8 and 7 mm.

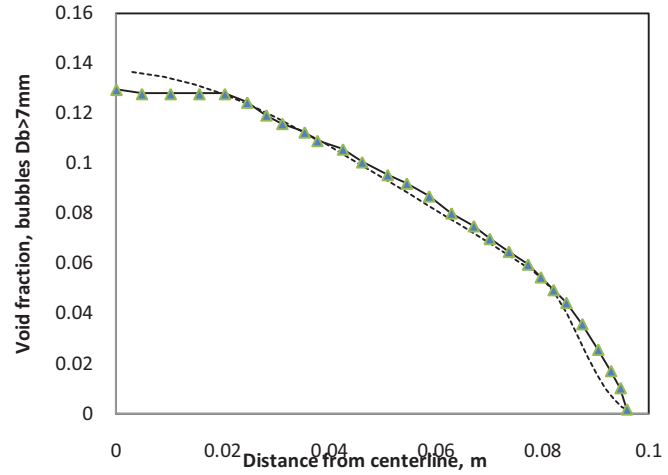

Figure 4(d). Radial distribution of volumetric concentration of bubbles having diameters larger than 7 mm.

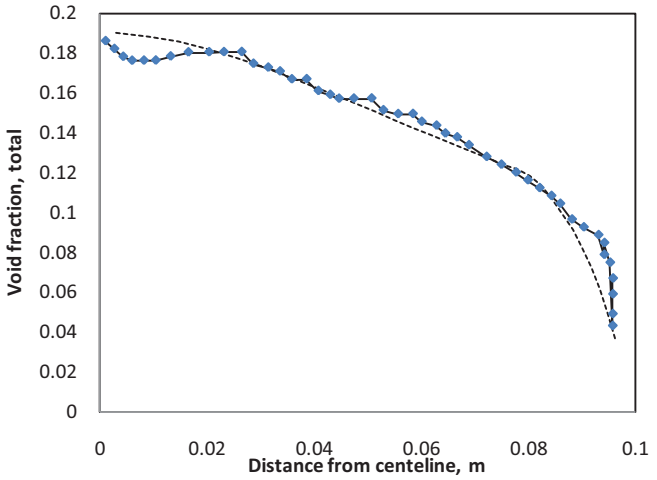

Figure 5. Radial distribution of gas void fraction; a comparison between predictions and measurements.

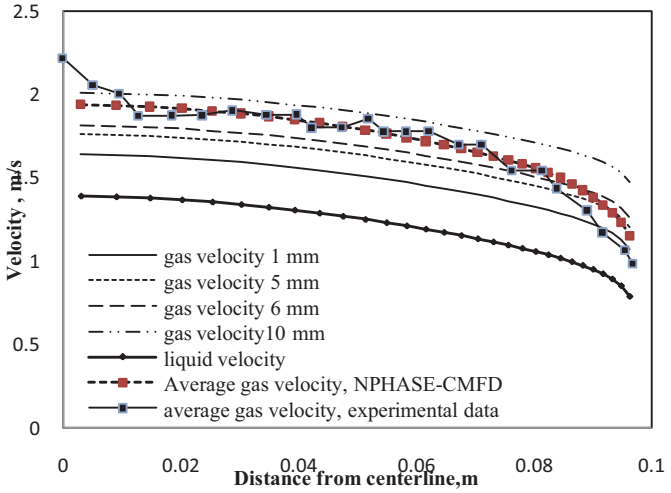

Figure 6. Calculated velocity distributions for liquid and each dispersed gas field, as well as the average gas velocity, compared against the average gas velocity measured in the experiments.

Parametric Study

(1) The effect of change of bubble diameter

The first parametric study was done to investigate the influence of bubble size on flow and phase distributions. Since two out of four dispersed bubble size groups determined experimentally are significantly wider than the other two groups, test calculations were performed to quantify the effect of the assumed bubble size on the results of predictions. Initially, the large bubble diameter was increased from 10 mm to 20 mm, and then the diameter of small bubbles was decreased from 3 mm to 1mm. The results of calculations are presented on Figures 7 and 8.

The average gas velocity shown in Figure 7 was defined using bubble volumetric fractions as weighing functions. As it can be seen, if the diameter of large bubble increases, the velocity not only increases, but also becomes more uniform. With the decrease of the small-bubble velocity, the profile also flattens, but the velocity magnitude decreases. This is because the major effect on flow in the axial direction is due to the drag force, which increases with decreasing bubble diameter. Hence, the bubbles are slowing down.

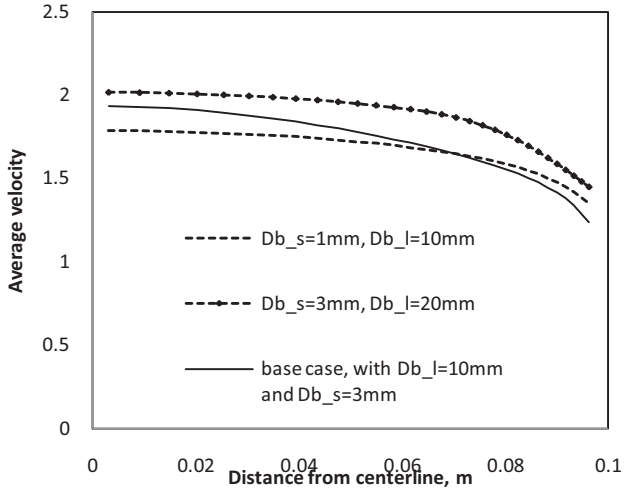

Figure 7. Effect of bubble diameter on radial distribution of the average axial gas velocity.

Figure 8 shows the radial distribution of cumulative gas void fraction. The gas fraction changes only slightly with decreasing size of small bubbles. On the other hand, increasing the average size of large bubbles considerably decreases the void fraction near the wall.

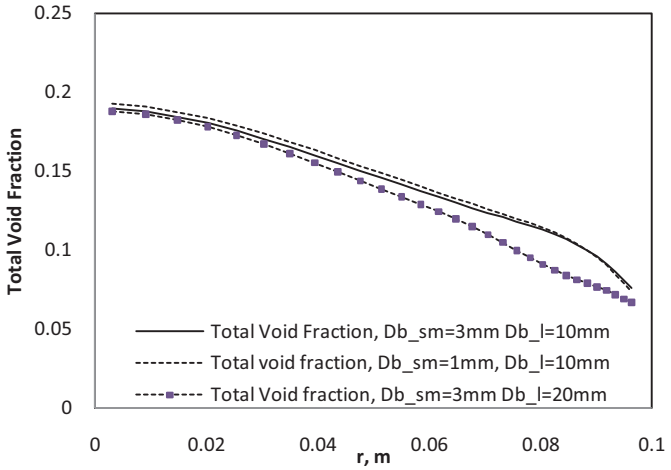

Figure 8. Effect of bubble diameter on radial distribution of gas volumetric concentration (void) fraction).

(2) The effect of computational grid

A grid optimization study was performed using a vertical circular tube. The effect of grid size and geometry was studied using meshes shaped as structured grids, equally-spaced in the axial direction. The total number of radial nodal points for each of the two grids tested was: 24 and 30, respectively. In the first case, the mesh was uniformly distributed in radial direction, whereas the second grid used a nonuniform radial spacing. The purpose of the comparison was to properly capture the effect of the wall on velocity and bubble concentration distributions. The numerical testing was performed by running the NPHASE-CMFD code using each grid for identical flow conditions. The objective was to check the impact on accuracy of predictions of both the number and size of radial nodes. The results are shown in Figures 9 and 10.

Figure 9 shows a comparison between the calculated radial distributions of the axial liquid velocity near the outlet of the pipe. As can be seen, the results for both grids are almost identical.

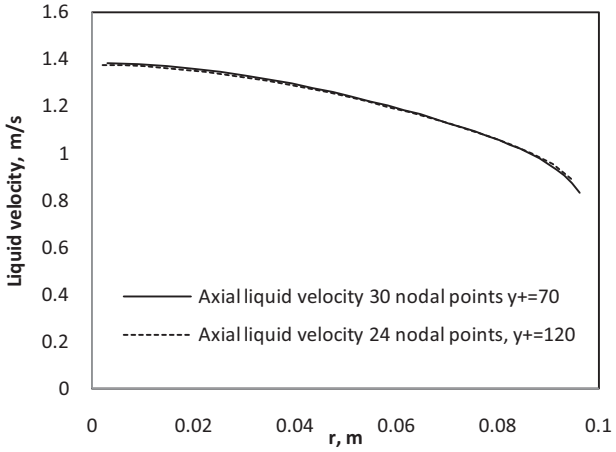

Figure 9. Radial distribution of axial liquid velocity, obtained for two different computational grids.

Figure 10 shows a comparison for the void fraction distributions along the radius near the outlet of the tube. The void fraction profiles are very close to each other. Thus, it has been concluded that both grids are sufficiently fine for the purpose of the present study.

(3) The effect of lift coefficient

According to observations of Tomiyama [1998], there is an inversion of the direction of the lift force at a certain critical bubble diameter, approximated at 5.8 mm for air/water flows at ambient conditions. As a result, in the case of upward flows small bubbles are pushed in the direction towards the pipe wall, while larger bubbles tend to move towards the center.

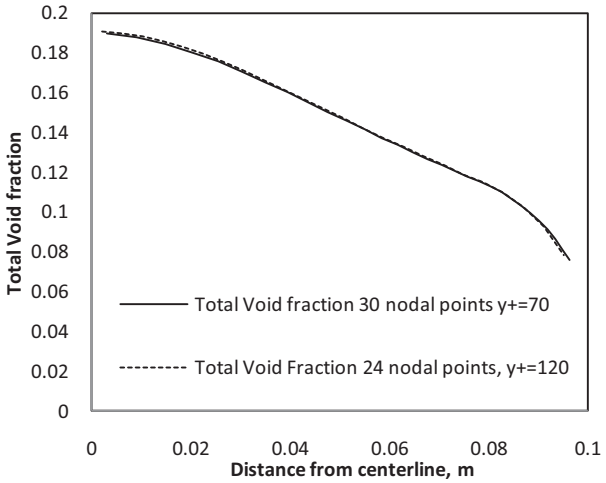

Figure 10. Radial distributions of total void fraction, obtained for two different computational grids.

Figure 11 shows the radial volume fraction distribution for large bubbles, d_b = 10mm, obtained for five different values of the lift coefficient for this bubble group, from $C_{l,4}$=0.1 to -0.1. This Figure shows how the distribution is affected by the change of lift coefficient from positive to negative. As expected, the corresponding maximum value of the volume fraction has moved from the wall to the center of the pipe.

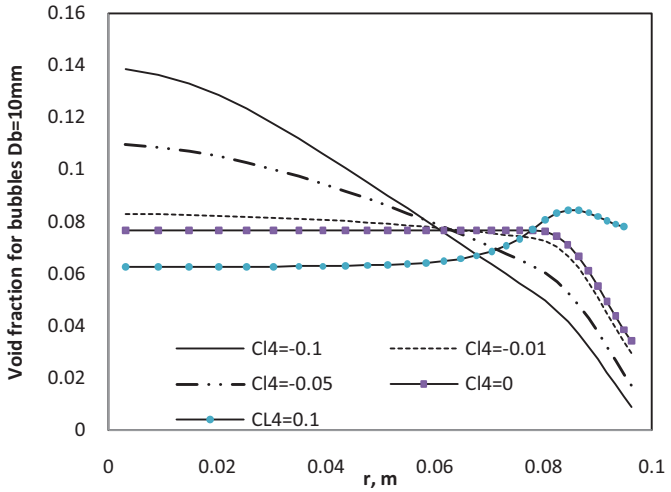

Figure 11. Radial void fraction profiles of large bubbles for different lift force coefficients.

(4) The effect of bubble-induced turbulence

Figure 12 shows the effect of the bubble-induced turbulence on gas velocity and total void fraction. As can be seen, when the effect of bubble-induced turbulence is neglected, there is some difference in the results close to the center of the tube due to a decrease in the total viscosity. However, the difference is small and the overall results are close to each other, showing that this effect is practically negligible for the flow conditions analyzed in this paper.

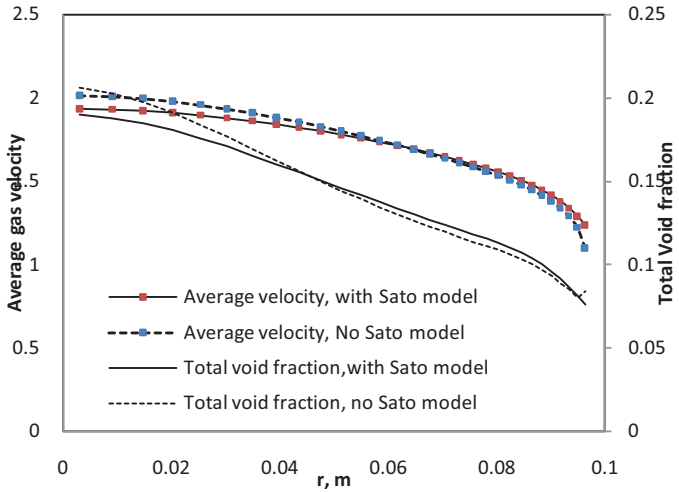

Figure 12. Effect of Sato model on the average gas velocity and void fraction distribution in radial direction.

CONCLUSIONS

The present work has achieved several objectives. One of them was to demonstrate the importance of proper physical closure modeling of two-phase flows in vertical conduits. In particular, selected computational and modeling issues have been investigated and resolved, associated with multi-dimensional simulations of multiphase flows using a multifield ensemble-averaged modeling framework. The model has been implemented in the NPHASE-CMFD solver and parametrically tested. The results of CMFD based computer simulations show both modeling and computational consistency. The results of calculations have been compared with the experimental data from the TOPFLOW test facility and a good agreement has been observed. Naturally, there are still unresolved modeling and computational issues which will require further investigation and additional work to be performed.

ACKNOWLEDGMENTS

The authors would like to acknowledge the financial and technical support provided by Idaho National Laboratory and the funding provided by the German Federal Ministry of Economics and Labor for the project which generated the experimental data used in the current work.

Funding for the computational work was supported by the U.S. Department of Energy, Office of Nuclear Energy, under DOE Idaho Operations Office Contract DE-AC07-05ID14517.

The experimental data were obtained in the frame of a current research project funded by the German Federal Ministry of Economics and Labor, project number 150 1329.

REFERENCES

Antal S.P., Ettorte S.M., Kunz R.F., Podowski M.Z., (2000) "Development of a next generation computer code for the prediction of multicomponent multiphase flows.", *Proceedings International Meeting on Trends in Numerical and Physical Modeling for Industrial Multiphase Flow*, Cargese, France.

Antal S.P., Podowski M.Z., Lahey R.T. Jr, Barber D., Delfino C. (2005), "Multidimensional Modeling of Developing Two-Phase Flows in a Large Adiabatic Riser Channel", Proceedings NURETH-11, Avignon, France.

Drew D.A., (1992) "Analytical modeling of multiphase flows", In: Lahey R.T. Jr in Boiling Heat Transfer, (Ed.: Lahey, R.T.Jr.), Elsevier, New York.

Lopez De Bertodano, M., (1992) "Turbulent Bubbly Two-Phase Flow in a Triangular Duct", PhD Thesis, Rensselaer Polytechnic Institute.

Lucas, D., Krepper, E., Prasser, H.-M., (2001) "Prediction of radial gas profiles in vertical pipe flow on basis of the bubble size distribution", Int. J. of Thermal Sciences, Vol. 40, pp. 217-225.

Lucas, D., Krepper, E., Prasser, H.-M., (2007) "Use of models for lift, wall and turbulent dispersion forces acting on bubbles for poly-disperse flows", Chem. Science and Engineering, Vol. 62, pp. 4146-4157.

Podowski M.Z., (2009) “On the consistency of mechanistic multidimensional modeling of gas/liquid two-phase flows”, *Nuclear Engineering and Design.,* doi:10.1016/j.nucengdes.2008.10.022.

Prasser H-M., Beyer M., Carl H., Gregor S., Lucas D., Pietruske H., Schutz P., Weiss F-P., (2007) “Evolution of the structure of a gas-liquid two-phase flow in a large vertical pipe”, *Nuclear Engineering and Design*, Vol. **237**,pp. 1848-1861.

Prasser, H.-M., Beyer, M., Carl, H., Manera, A., Pietruske, H., Schütz, P., (2007a). “Experiments on upwards gas/liquid flow in vertical pipes”, *Report FZD-482*.

Sato Y., Sekoguchi K. (1975) Liquid velocity distribution in two-phase bubble flow, *Int. J. Multiphase Flow*, Vol.**2**, 79-95.

Tomiyama, A. (1998). “Struggle with Computational Bubble Dynamics”. *Proceedings International Conference on Multiphase Flow*, Lyon, France.

Wallis G.B., (1969), “One Dimensional Two Phase Flow”, New York: Mc Graw-Hill.